

Synthesis, Characterization and Hydrogen Absorption Study of Silver-Gold Porous Bimetallic Nanoalloy

By

Maham Hayat



A dissertation submitted in partial fulfilment of requirements for the
Degree of Master of Science in Chemistry

Supervised by

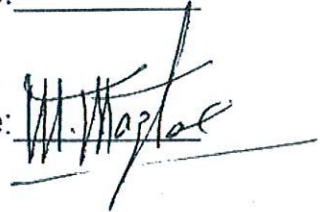
Prof. Muhammad Mazhar

Department of Chemistry
School of Natural Sciences
National University of Sciences and Technology
Islamabad, Pakistan
2020

National University of Sciences & Technology

MASTER THESIS WORK

We hereby recommend that the dissertation prepared under our supervision by: Maham Hayat Regn No. 00000203172 Titled: Synthesis, Characterization and Hydrogen Absorption Study of Silver Gold Bimetallic Nanoalloy be accepted in partial fulfillment of the requirements for the award of MS degree.

Examination Committee MembersName: Dr. Mudassir IqbalSignature: Name: Dr. Manzar SohailSignature: External Examiner: Dr. Rohama GillSignature: Supervisor's Name: Prof. Muhammad MazharSignature: Co-Supervisor's Name: Dr. Asad MumtazSignature: 

 Head of Department

08/9/2020
 Date
COUNTERSIGNEDDate: 08/9/2020

 Dean/Principal

THESIS ACCEPTANCE CERTIFICATE

Certified that final copy of MS thesis written by Maham Hayat, (Registration No. 00000203172), of School of Natural Sciences has been vetted by undersigned, found complete in all respects as per NUST statutes/regulations, is free of plagiarism, errors, and mistakes and is accepted as partial fulfillment for award of MS/M.Phil degree. It is further certified that necessary amendments as pointed out by GEC members and external examiner of the scholar have also been incorporated in the said thesis.

Signature: _____



Name of Supervisor: Dr. Muhammad Mazhar

Date: _____

Sept. 08, 2020

Signature (HoD): _____



Date: _____

08/09/2020

Signature (Dean/Principal): _____



Date: _____

08-09-2020

In the Name of Almighty ALLAH, The most Beneficent

And the most Merciful

Dedicated to my loving grandparents, parents, siblings

And Dr. Sikandar Hayat

Acknowledgments

First, all praise to the Almighty Allah for providing the strength, opportunity and ability to commence and complete this research successfully. During the completion of my degree, I have met several people without whom I could not have achieved this.

*In this journey towards the degree, I have found a true researcher, advisor, teacher and a pillar of support as my thesis supervisor, **Prof. Muhammad Mazhar**. He provided his constant support and guidance and invaluable suggestions during my research. He allowed me to pursue this research with complete freedom, while silently ensuring that I do not deviate from the course of my research.*

*I am thankful to my GEC members, **Dr. Manzar Sohail** and **Dr. Mudassir Iqbal** for their support, encouragement and credible ideas. I pay cordial thanks to my co-supervisor, **Dr. Asad Mumtaz** who motivated me at all times. I feel pleasure to pay a special thanks to the HoD Chemistry, **Dr. Muhammad Arfan**, to the School of Natural Sciences for the financial support during my MS research. I greatly acknowledge the facilities and technical support provided by other schools at NUST like USPCASE and SCME. I would like to express my gratitude to the Department of Environmental Chemistry at Fatima Jinnah Women University, Rawalpindi for their support.*

A precious thanks to my research fellows and other batch mates for their immense help in my research work. My acknowledgment would be incomplete without thanking my biggest support, my family for their unwavering support at all times.

Maham Hayat

Abbreviations and Symbols

NA	Nanoalloy
AgAu	Silver Gold
Fcc	Face-centered cubic
XRPD	X-ray Powder Diffraction
SEM	Scanning Electron Microscopy
IR	Infra-Red
MOFs	Metal Organic Frameworks
BET	Brunauer-Emmet-Teller
TGA	Thermogravimetric Analysis
DTA	Differential Thermal Analysis
FWMH	Full Width at Half Maxima

Abstract

Keeping in view the recent advances in hydrogen energy and the lack of efficient hydrogen storage materials, a bimetallic porous nanoalloy has been synthesized by the inverse-Leidenfrost method. The prepared alloy was characterized using XRPD, SEM/EDS, FTIR and TGA. The comparison of XRPD data with the standards shows the presence of both Ag and Au in the nanoalloy while the SEM micrographs clearly show the porous morphology having structural defects that can absorb hydrogen. The hydrogen absorption studies were performed at low temperature of -78°C using vacuum line fitted with nitrogen and hydrogen gas. The weight percent of absorbed hydrogen was determined by the loss in weight percent by TGA. A loss of approximately 2.95% demonstrates that the nanoalloy can be used as a benign shock-proof and hazard free hydrogen storage material for energy applications. This nanoalloy can provide a catalytic design for the future hydrogen storage materials.

Table of Contents

INTRODUCTION.....	1
1.1 Preparative methods for Alloys	1
1.2 Solid Solutions.....	1
1.2.1 Complete Solid Solubility	2
1.2.2 Partial Solid Solubility	2
1.2.3 Substitutional Solid Solutions	2
1.2.4 Interstitial Solid Solutions	3
1.2.5 Intermetallic Compounds	3
1.3 Types of Alloys	4
1.3.1 Substitutional Alloys	5
1.3.2 Interstitial Alloys.....	5
1.3.3 Transformational Alloys	6
1.4 Hydrogen Energy.....	7
1.5 Nanoalloys	8
1.6 Leidenfrost Effect.....	9
1.7 Characterization Techniques	10
1.7.1 Infrared Spectroscopy	10

1.7.2	X-ray Diffraction.....	10
1.7.3	Scanning Electron Microscopy (SEM)	11
1.8	Thermogravimetric analysis (TGA)	13
1.9	Aim and Motivations	14
2	LITERATURE REVIEW	15
2.2	Metal Nanoparticle synthesis by Partial Film Boiling Method	18
2.3	Leidenfrost Approach-Green Chemistry	19
2.4	Inverse Leidenfrost Effect for Nanoalloy synthesis	20
2.5	Use of Porous Nanoalloys for Energy Storage and Conversion.....	20
2.6	Use of Ag-Au Nanoalloys as Catalysts	20
2.7	Optical Properties of AgAu NPs	21
3	EXPERIMENTAL.....	23
3.1	Experimental.....	23
3.1.1	Materials.....	23
3.2	Preparation of H _{Au} Cl ₄	23
3.3	Synthesis of Macroporous AgAu Nanoalloy:.....	24
3.4	Hydrogen Absorption Capacity	26
4	RESULTS AND DISCUSSIONS.....	27

4.1	Hydrogen as an Alternate Energy Source:	27
4.2	XRPD Results.....	28
4.3	SEM Results	30
4.4	FTIR Analysis.....	32
4.5	Thermogravimetric (TGA) Analysis	34
4.6	Conclusion.....	37

List of Tables

Table 1 Interstitial Alloys Vs Substitutional Alloys..... 6

Table 2 List of Alkali and Alkaline Earth metals with their Hydrogen Storage Capacities..... 17

List of Figures

Figure 1: Formation of Solid Solution and Intermetallic Compound upon alloying metals. Reproduced with permission from Ref. [1].	4
Figure 2 Phase diagram for Silver-Strontium (Ag-Sr) system showing intermediate phases. Reproduced with permission from Ref. [9]	7
Figure 3 A drop of liquid held up by the vapour phase depicting Leidenfrost Effect. Reproduced with permission from Ref. [19]	10
Figure 4 Applications of AgAu NAs	22
Figure 5 (a) Aqua Regia prepared to dissolve gold metal (b) Preparation of H _{Au} Cl ₄ from gold	23
Figure 6 Step-by-step synthesis of AgAu NA	24
Figure 7 (a) Schlenk tube filled with AgAu sample under vacuum (b) Schlenk tube with AgAu sample submerged in Acetone/Liquid Nitrogen mixture	26
Figure 8 XRD patterns for AgAu alloy obtained after fine grinding	28
Figure 9 SEM images obtained for AgAu Nanoalloy at various magnifications (a) shows the overall morphology of the alloy with porous structure (b) a closer view showing large structural defects (c) size of the pore in nm range (d) large structural defect of 142 nm visible	31
Figure 10 SEM micrograph of AgAu NA with EDX spectrum	32
Figure 11 FTIR Spectrum of AgAu NA obtained after sintering at 500°C	33

CHAPTER 1

INTRODUCTION

An alloy is a homogeneous mixture of two or more metals. Alloys exhibit different properties than their pure metal counterparts. [3] Alloys have been considered as materials of high strength and importance just like the noble metals, silver and gold. The first ever alloy that has been used since centuries was bronze. Bronze is an alloy of copper and tin but comparably harder than tin. These improved properties of bronze were incorporated in making tools and weapons.

1.1 Preparative methods for Alloys

Alloys can be synthesized using various methods and approaches, some of which are described below:

- a) Melting the metals and mixing them together has been the most common method to synthesize alloys.
- b) Mixing and grinding together the alloy ingredients can be also be used to synthesize the alloys
- c) From the salt solutions- the metal salt solutions can be subjected to electrolysis to achieve the alloy formation.
- d) Reduction of metal oxides can also yield alloys.

When metal atoms are mixed together to form alloys, formation of a solid solution occurs. This solid solution maybe a partially soluble solid solution or a completely soluble depending upon the nature of the metal atoms.

1.2 Solid Solutions

Alloys can have broad composition ranges. These compositional phases can be referred as the crystal impurities within the alloys. When a large number of impurities enter the crystal structure without altering the structure of the crystal, solid solution is formed. The defects in the crystals maybe intrinsic if they arise from the stoichiometric crystals. On the other hand, the crystal defects can be extrinsic if they arise due to certain impurities or doping. If the concentration of the doped material rises above than 0.1-1%, the materials formed are referred

to as Solid solutions. In other words, a solution with variable composition maybe termed as a solid solution. Solid solutions in binary systems can be classified as complete solid solutions as well as partial solid solutions on the basis of their limits of solubility in one another. Solid solutions can be substitutional solid solutions and interstitial solid solutions depending upon the way in which the impurity atoms sit in the crystal lattice. Binary systems may show complete or partial solid solubility.

1.2.1 Complete Solid Solubility

A complete solid solubility occurs when the binary system shows complete miscibility in both liquid and solid states. In a binary system, containing A and B as the components, the melting point of one member maybe depressed or increased by the addition of the other member. Upon cooling such a solution, complex pathways appear that result in different compositions.

1.2.2 Partial Solid Solubility

Complete solid solubility is observed when the anions and cations replacing each other in the crystal structure have the same size and possess the same crystal structure. However, the metal atoms can be partially soluble in each other. In a binary system containing A and B as two components, A can be partially soluble in B and vice versa. The extent of solid solution formation for such a system is maximum at a point called the eutectic point. The two types of solid solutions formed on the basis of composition are:

1.2.3 Substitutional Solid Solutions

A substitutional solid solution between two similar elements is formed when an atom or ion in the parent crystal structure is replaced by another atom or ion at the same point. [4] A large number of physical and chemical properties determine the formation of a substitutional solid solution between two metals. Hummay-Ruthray studied a large number of alloy systems in the 20th century to understand the principles of alloy formation [5]. The probability of formation of a solid solution between two metals can be predicted by the Hummay-Ruthray rules. These rules hold good for the substitutional solid solutions. The substitutional solid solutions can be further classified as random, clustered or ordered substitutional solutions depending upon the arrangement of impurity atoms within the parent structure.

For example, in the Copper-Nickel system, both Cu and Ni possess the same crystal structure as face centered cubic (Fcc), thus showing complete solid solubility. Copper atoms may randomly substitute the Nickel atoms and vice versa to form a substitutional solid solution. The oxides Al_2O_3 and Cr_2O_3 undergo solid solution formation when reacted together. The properties of the Al_2O_3 - Cr_2O_3 system change considerably upon doping as Al_2O_3 is white but upon the substitution of Cr^{+3} impurity, red colour is imparted. Thus, it is evident that a small impurity can have significant effect on the properties. The substitutional solid solutions possess low thermal and electrical conductivities as compared to their parent metals but they are stronger and harder than their metal counterparts. [6] On a wider perspective the substitutional solid solutions can be further categorized into; homovalent and heterovalent or aliovalent substitutional solid solutions. In homovalent substitutional solid solution, ions which are replaced by new ions carry the same charge thus, no extra charge carriers are required to balance out the overall charge on the crystal lattice. For example, in the case of Al_2O_3 - Cr_2O_3 system, since both Al and Cr possess +3 oxidation state. For aliovalent or heterovalent solid solution, to compensate the charges, electrons, holes or vacancies are required. [7]

1.2.4 Interstitial Solid Solutions

For substitutional solid solutions the metals should have comparable atomic radii. In the case of interstitial solid solutions, the atomic radius of impurity atom should be at least half as compared to the parent atom. Interstitial solid solutions are formed when the added foreign atom sits in the empty spaces in the crystal structure called as “interstices” or voids. Such solutions are produced when small impurity atoms like H, C or N incorporate themselves into the metal structure [1]. The Pd metal forms an interstitial solid solution with hydrogen H. Pd has an fcc structure with hydrogen occupying the interstitial spaces to form the metal hydride. This product is the interstitial solid solution as PdH_x $0 \leq x \leq 0.7$. Another important example of an interstitial solid solution is the one in which C sits in the octahedral sites of fcc iron to form steel, an important alloy of commercial importance.

1.2.5 Intermetallic Compounds

The metal atoms upon combination give rise to form a new compound having distinct properties known as intermetallic compounds. Intermetallic compounds are hard and brittle and impart strength to the alloy. Alloys are not necessarily composed of one phase rather they can have

multiple phases. In the case of Al-Cu alloy, Al combines with Cu to form an intermetallic compound. The alloying process to yield solid solution and intermetallic compound has been described by the figure 1. Three different metals (A, B, C) undergo alloy formation. Metal A can replace metal B or vice versa to form a substitutional solid solution. C possessing small sized atoms can easily fit into the interstices of the metal B to form an interstitial solid solution. If however, C replaces the atoms of B it produces an intermetallic compound with distinct properties than either A, B or C. [1]

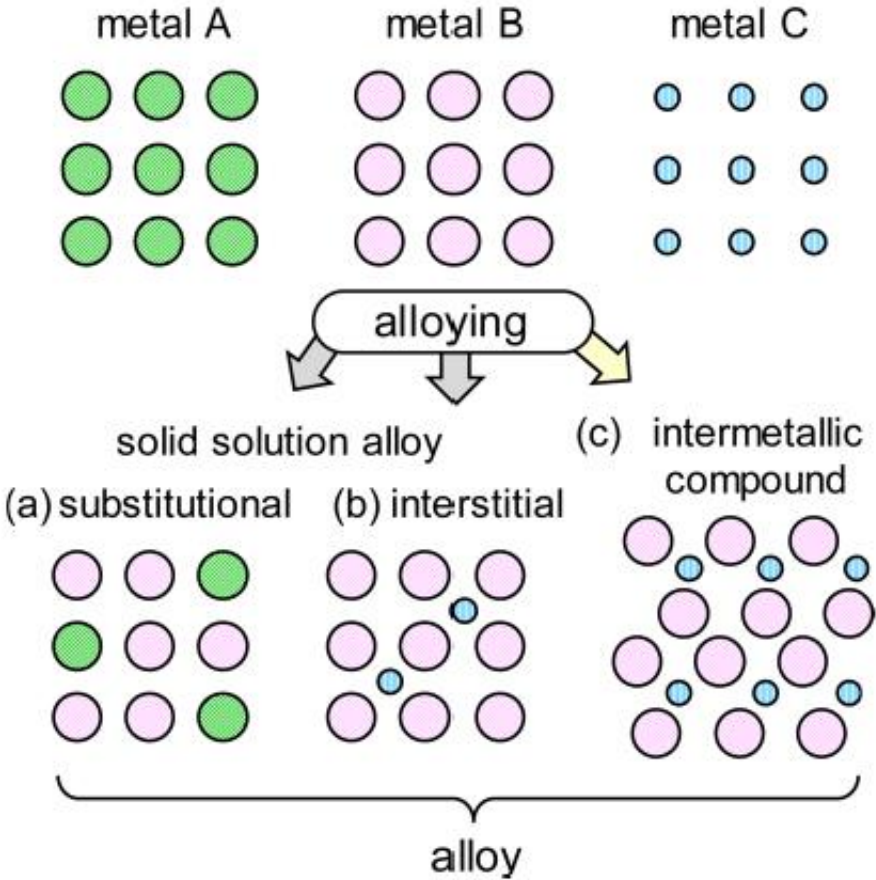


Figure 1: Formation of Solid Solution and Intermetallic Compound upon alloying metals. Reproduced with permission from Ref. [1].

1.3 Types of Alloys

Alloys can be categorized in a number of different classes depending upon their compositions, phases, structures, properties, applications etc. the alloys can be classified into:

1.3.1 Substitutional Alloys

In this type of alloys, the solvent atoms in the crystal lattice are replaced by the solute atoms without rendering any structural changes (Fig. 2). Such alloys are formed using elemental metals such AgAu, AgCu etc. the alloy formation is governed by the Hume-Rothery rules.[8].

a) Crystal Structure Rule

The elements forming the solid solution must have identical crystal structure

b) Atomic Size rule/ the 15% rule

There should not be a difference of more than 15% in the atomic sizes of the elements forming a substitutional solid solution. Limited solubility occurs if the difference is >15%. The empirical rule can be shown as:

$$\text{Mismatch} = \left[\frac{r(\text{solute}) - r(\text{solvent})}{r(\text{solvent})} \right] \times 100 \leq 15\%$$

c) The Electronegativity Rule

The difference in electronegativity between the two elements should be low

d) The Valence Rule

The elements must possess the same valence i.e. the elements must belong to a same group of the periodic table.

1.3.2 Interstitial Alloys

These alloys are formed when the solute atoms instead of occupying the lattice sites reside in the crystallographic pores of the lattice structure. Small atoms such as B, C, and H are usually incorporated in the metal structure to render useful properties. The key differences among the interstitial alloys and substitutional alloys can be summarized as:

Table 1 Interstitial Alloys Vs Substitutional Alloys

Interstitial Alloys	Substitutional alloys
They are produced when small atoms fill the interstices or empty spaces in the metal structure.	When one metal atom substitutes another metal of the same size within the crystal structure, substitutional alloys are produced.
Formed by small atoms of different elements.	Formed by metal atoms of same or similar sizes.
Interstitial mechanism is involved in the formation of such alloys.	Atom exchange mechanism leads to the formation of substitutional alloys.
Fe and C produce an interstitial alloy known as steel.	Bronze and Brass are the classic examples of substitutional alloys.

1.3.3 Transformational Alloys

Intermetallic compound formation leads to transformational alloying. When a strong chemical bond exists between the metallic atoms, intermediate phases are produced. Such compounds are distinct from their parent solutions and possess a different crystal structure. They possess a highly ordered structure and good mechanical and physical properties. The intermediate phases are described as:

1.3.3.1 Intermediate Phases

Often when metals are mixed together, they may possess different crystal properties than the pure solutions, such new structures formed are called Intermediate phases. The *intermediate phases* exist between the metal components e.g. Fe_3C , Al_3Ni and CuAl_2 are some of the intermetallic compounds formed among the metals. The figure 2 shows a phase diagram between Sr and Ag. Both metals form a number of intermediate compounds which have lower free energy as compared to the mixture of the phases. However, it is evident from the phase

diagram that the intermediate phase undergoes melting without any change in its state. This type of behaviour is termed as congruent melting. These phases are thermodynamically stable because they are formed at a lower free energy than the two forming-components. They have unique melting points like the pure components. According to phase diagrams, the metals forming such compounds are called “parent phases” and the products are called “intermediate phases”. An Intermediate phase may melt congruently or incongruently if it melts without any change in its state or may change into some other physical state before melting respectively. [6]

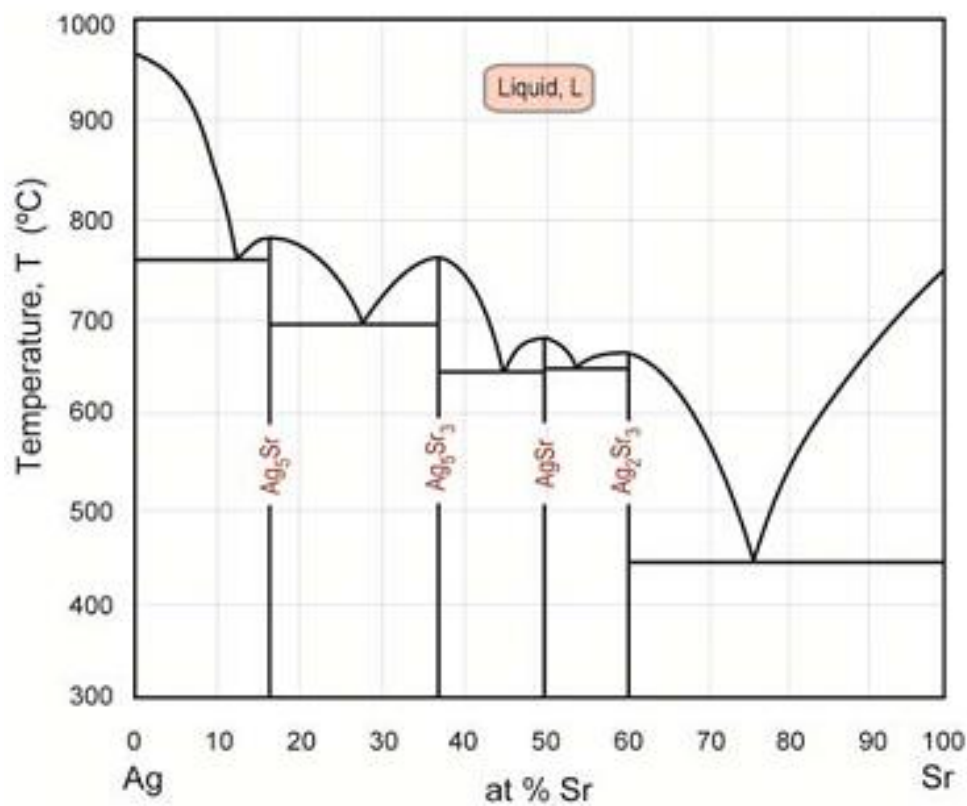


Figure 2 Phase diagram for Silver-Strontium (Ag-Sr) system showing intermediate phases. Reproduced with permission from Ref. [9]

1.4 Hydrogen Energy

The depletion of non-renewable energy sources like fossil fuels lead to the discovery of renewable energy sources like wind, tides and solar energy. These sources are environmental friendly and infinite in the nature. Most of the scientists agree on the using hydrogen as a source of energy and fuel in the near future since it is a high energy, low emission and non-polluting

fuel source [10]. Hydrogen is an important energy carrier. It can be stored in fuel cells to transport energy and can be converted it into other useful sources such as electricity. The use of hydrogen as a fuel may revolutionize the energy needs of the world and is emerging as “hydrogen economy”. Although hydrogen is an efficient fuel source yet the problem of storage of hydrogen to be used as a fuel persists due to its low energy density and light weight than all the elements. [11] Presently, a small amount of hydrogen storage materials have been designed to effectively store and produce hydrogen such as metal organic frameworks, porous alloys, metal hydrides, porous carbons etc.

1.5 Nanoalloys

Metal nanoparticles (MNPs) and Nanoalloys (NAs) have been used since centuries. The famous Lycurgus Cup of the 4th Century AD was made of Ag and Au nanoalloy particles [12]. Multimetallic and bimetallic Nanoalloys have attracted much attention due to their easily controllable properties in the Nano range. NAs possess tuneable physical and chemical properties and varying morphology, shape and size. The properties of bimetallic NAs are significantly different from pure metal nanoparticles. McNamara et.al has defined nanoalloys as an alloy formed by the dispersion of NPs of two or more metals and investigated the biomedical applications of a number of NAs [13] . Metal nanoparticles and nanoalloys are synthesized using various techniques and from different media i.e. gas phase, solution or matrix etc. [14] One of the common methods used to synthesize NAs is by reducing the metal salts. The reduction is carried out in the presence of a suitable surfactants such as citrates or thioethers etc. Salt solutions containing individual metals are subjected to reduction to form the metal NAs and MNPs. The catalytic ability of certain metals can be improved by alloying thus this makes NAs very popular catalysts. Another important advantage of NA catalysts is the use of cheap metals such as Fe, Ni, Co etc. which possess the same or even better properties than the expensive and rare metals like Pt and Ir. Pt, Ir and Re bimetallic NA catalysts find applications in petrochemical reforming while Pd-Au NAs are found to catalyse numerous chemical reactions such reduction of alcohols and CO and acetylene cyclomerization.[15]. For over 50 years, the bimetallic NAs are being employed as electrocatalysts.[16]. NAs of Ru-Pt can be used to remove CO as an impurity from Hydrogen in fuel cells.

1.6 Leidenfrost Effect

In 1756, *Johann Gotlob Leidenfrost* observed the boiling of small droplets of liquid on a hot surface. The liquid droplet floated on the hot surface without boiling since the hot surface was at a much higher temperature as compared to the boiling point of the liquid [17]. A vapour layer is formed between the hot surface and the droplet, levitating it. This prevents evaporation until it is dried completely at its Leidenfrost Temperature. As a result, temperature gradient is formed between the droplet and the vapour layer. In the case of a water droplet, this temperature gradient causes the ionization of the water to hydronium ions (H_3O^+) and hydroxyl ions (OH^-). Using the same principle, many metals undergo reduction. In the case of water, the Leidenfrost phenomenon is observable at 200°C or higher temperatures.[18] This phenomenon is commonly observable when water droplets are placed on a super-heated frying pan. The particles or droplets rapidly move about the surface without “wetting” it ultimately being evaporated. The fig. 3 demonstrates the Leidenfrost effect in which a drop of liquid is being held up by the vapour phase formed between the hot surface and the drop [19]. The Leidenfrost method/effect has also been called as the Film Boiling Phenomenon. Another important phenomenon which was discovered by Faraday (1828), explains that when a hot body is placed into liquid with a comparably low boiling point, a layer of vapour is formed around the hot body [20]. Similarly, if a hot liquid droplet is placed upon the surface of a cold liquid, it levitates due to the formation of a vapour layer in between them, this phenomenon is referred to as Inverse Leidenfrost Effect. [21] In such cases, the liquid droplet causes the substrate to evaporate without any change in its own mass.

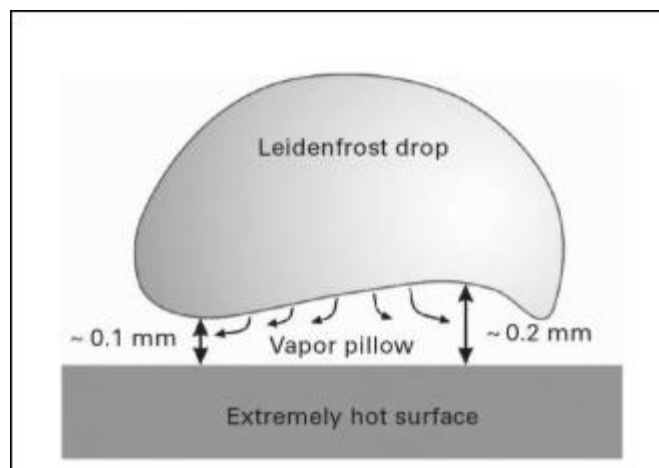


Figure 3 A drop of liquid held up by the vapour phase depicting Leidenfrost Effect.
Reproduced with permission from Ref. [19]

1.7 Characterization Techniques

The various properties of the samples such as morphology, size, pore structure, composition etc. were thoroughly studied using various analytical techniques. The following section describes briefly the working principle and instrumentation for these techniques.

1.7.1 Infrared Spectroscopy

Infrared spectroscopy is the analytical technique used to analyse the samples based on their atomic vibrations thus, also known as “Vibrational Spectroscopy”. Nearly all types of materials, solids, liquids, mixtures etc. can be analysed with IR. Infrared radiation upon passing through the sample are absorbed at various frequencies which is shown on the infrared spectrum. The irradiated atoms undergo excitations to higher energy levels and these excited atoms upon de-excitation emit photons of the characteristic wavelength. The IR spectra is a plot of this wavelength vs absorbance or transmittance. The molecules which show a changing dipole moment are infrared active upon passing IR. For this analysis, IR in the range of $4000\text{-}400^{-1}$ cm is used. In the case of inorganic compounds particularly, the IR absorption occurs at lower wavelengths. [22]

1.7.2 X-ray Diffraction

X ray diffraction is a powerful analytical technique used to analyse the physio-chemical features

of the crystalline as well as powdered substances. Sample properties such as crystallinity, particle size, polymorphism, phase transitions can be estimated using X-ray diffraction. This technique works on the principle of X-ray diffraction from the crystal surface.

The commonly used X-ray for diffraction is the $K\alpha$ emitted from Cu having a wavelength $\lambda = 1.5418 \text{ \AA}$. The crystals behave in the same way as the diffraction grating to diffract X-rays. The diffraction phenomenon has been thoroughly explained by the Bragg's law. According to this law, the structure of the crystal can be depicted as made of layers or planes. When an X-ray is incident upon the crystal it may be reflected back at the same angle but some x-rays penetrate the top layers and are diffracted from the bottom layers. These diffracted layers cover an extra distance which is equal to the crystal spacing between the two layers denoted as " d ". When the reflected beams undergo constructive interference, we observe the phenomenon of X-ray diffraction. However, it will occur only when the d -spacing is the integral multiple of the wavelength as mentioned in the Bragg's law below,

$$n\lambda = 2d\sin\theta$$

Where n represents an integer as (1, 2, 3...), λ represents wavelength of the incident beam, θ is the diffraction angle and d is the perpendicular distance between two adjacent planes. [23]

The monochromatic X-ray beam is focussed on the crystalline sample to find out its structural parameters. Typically, a cathode-ray tube (CRT) produces polychromatic X-ray beams. These beams are then filtered through a monochromator to produce the monochromatic X-rays which ultimately fall on the sample planes. An electric current of 15-60 kV is used to produce electrons which hit the metal source such as Cu, Cr, Mo, Ag or Fe to produce X-rays. These X-rays pass through a collimator and fall on the sample. Several phenomena such as diffraction, scattering, refraction are observed upon interaction of X-rays with the sample. This interaction can be obtained on an x-ray spectrum.

1.7.3 Scanning Electron Microscopy (SEM)

Scanning electron microscopy is analytical instrument that gives information regarding the morphology, surface topography, crystalline properties and chemical composition etc. of the material. The first scanning electron microscope dates back to 1938 invented by Manfred von Ardenne [24]. The electron beam used in the SEM has several advantages over the optical

microscope as it gives a detailed three dimensional image of the sample. The SEM consists of an electron source, electromagnetic condenser lens followed by the objective lens, a sample stage, scanning coils, electron detector and an operating system [25]. The general configuration of the SEM is given below:

a) Electron Source

For SEM, a stable electron source is required that can produce an electron beam of high energy (2-40 keV). Three types of electron guns are particularly used in SEM. The most common type is the tungsten filament which produces electrons upon heating at 2500 °C. Lanthanum Hexaboride (LaB₆) also produce electrons in the same way but the beam is brighter [26]. Thus, making these filaments expensive. The new SEMs are equipped with field emission sources to produce high energy electron beams.

b) Condenser and Objective Lenses

SEM uses pair of electromagnetic condenser and objective lens to control the size and the speed of the electron beam. These lenses collimate the electron beam into a parallel stream to be focused on the sample. The electron beam penetrates up to 1 μm in the sample.

c) Specimen Stage

The sample to be analysed is placed on the stage. The stage should be smooth and clean to ensure high resolution images. It can be moved horizontally, vertically or even rotated to get a better view of the sample.

d) Electron Detector

The sample is ionized when the incoming electron beam knocks out the outer shell electrons. These loosely bound electrons of low energy (3-5eV) are called as secondary electrons. These electrons accurately show the position of the beam on the sample and give a clear topographic picture. These electrons further produce light upon collision with the fluorescent material. This light signal is amplified and converted into electric signal.

e) Image Display Unit

The amplified signals from the secondary electron detector are fed to the display unit. Earlier,

a cathode ray tube (CRT) functioned as a display unit but now liquid crystal displays are employed. The scan speed of the electron probe can be varied in several steps, a slow scan speed helps to obtain and save the images of the sample whereas a fast scan rate can be used to observe.

1.8 Thermogravimetric analysis (TGA)

The thermal analysis TA, is the study of physical and/or chemical properties of the material with the changes in temperature. TA includes techniques as *thermogravimetric analysis TGA*, *differential thermal analysis (DTA)*, *differential scanning calorimetry (DSC)* and *thermomechanical analysis (TMA)*. Since all the solids are thermally active to some extent so TA can provide useful information about them. In TGA, the sample undergoes a mass change when subjected to programmed heating or cooling. This mass change is recorded as a function of temperature or time [27]. TGA is helpful in studying the thermal process such as oxidation/reduction, sublimation, decomposition etc. however, only the thermal events that lead to a mass change can be studied using TGA. A thermobalance is the most important part of a TGA instrument. It has further subunits; a microbalance, sample pan, furnace, temperature controller and recorder/plotter [28]. The instrumentation for TGA is:

a) Microbalance

It is an important component of the thermobalance and records the changes in the mass of the sample. Several types of microbalances can be used that include null-type and deflection type microbalances.

b) Sample Pan

The sample under study is placed in a sample holder or sample pan also known as the crucible, attached to the microbalance. Generally, crucibles of varying size, shape and materials are used in TGA. Aluminium, quartz and platinum are some the materials employed in making crucibles. The shape or type of the crucible used depends on the heating conditions. The crucible should have high thermal stability and it should efficiently and uniformly distribute the heat to the sample above.

c) Furnace

A furnace is used to maintain a linear heating rate in the chamber. The crucible is placed inside this hot zone. Heating coils of variable temperature ranges are employed according to the desired temperature e.g. tungsten, nichrome wire, graphite etc. the furnace material should make no magnetic interaction with the sample as it can lead to the changes in the mass of the sample.

d) Temperature Sensor

The temperature is measured with a thermocouple. Thermocouples made of Chormal or Alumel can measure temperatures up to 1100 °C while thermocouples made of tungsten are used to measure temperatures higher than 1100 °C. The position of the thermocouple is very important in determining the temperature of the sample and crucible accurately.

e) Temperature Programmer

The temperature can be easily controlled using the temperature programmer. The heating rate can be increased or decreased during the analysis. The temperature change may be recorded on Fahrenheit or Celsius scale against time.

f) Data Recorder

A microcomputer is attached with the thermobalance to measure and chart the output. The weight loss is plotted as a curve against temperature.

1.9 Aim and Motivations

The bimetallic nanoparticles and nanoalloys of metals like Ag and Au have emerged as promising materials because of their improved chemical stability and high catalytic activity. The porosity inculcated in these alloys can be applied to store hydrogen in it [29]. In this way these materials can act as efficient sources of hydrogen absorption/desorption. Inverse-Leidenfrost method is an economical and straightforward method to synthesize porous nanoalloys. The key goal of this research is to synthesize the NAs of Ag-Au through the solution chemistry approach and employing the inverse Leidenfrost method. The reaction conditions will be optimized for the reduction of salts. After this, hydrogen absorption study will be performed to investigate the storage of hydrogen

Chapter 2

LITERATURE REVIEW

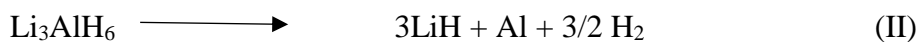
2.1.1 Materials for Hydrogen Storage

The non-renewable energy sources like fossil fuels will soon be depleted, therefore the world is looking for alternative energy solutions to tackle the energy needs. It has been estimated that with the current rate of consumption our natural gas and coal resources will deplete in the next 70 and 200 years respectively [30]. In this case, the hydrogen energy will be an effective candidate among all other sources such as the solar energy, wind energy, geothermal energy etc. mainly because hydrogen is abundantly available in the environment, produces no toxic by-products and has the highest energy density of 120 MJ/kg. The research for effective hydrogen storage materials is being pursued since a decade with a few materials able to store and produce hydrogen at ambient conditions. The Hydrogen Economy aims at storing the electricity through the chemical bonds of hydrogen. Materials based hydrogen storage is the only safe and economical option to use hydrogen as a fuel in the future [31]. Hydrogen can be stored via physisorption which includes the physical sorption of the gas in the pores of the materials such as the porous carbons or other porous alloys. In the case of chemisorption or chemisorption materials like hydrides would be effective. Weak binding forces of 4-10 kJ/mol are involved in physisorption while in chemisorption strong binding forces of 50-100 kJ/mol operate [32]. In the case of MOFs, porous carbons and zeolites, the hydrogen is physically sorbed in the pores of the materials. This phenomenon depends upon various factors such as the pore size, pore volume, surface area of the material [33]. The solid-state storage materials for hydrogen present increased safety, higher storage capacities and energy efficiency over the conventional storage methods [34].

Metal organic frameworks are defined as the class of materials containing metal ions coordinated with organic ligands. The careful substitution of these ligands renders useful important properties like increased surface area and porosity, which can effectively uptake hydrogen in them. MOFs have been used since over a decade now to store hydrogen in them. The open pore structure of the MOFs makes adsorption and desorption of hydrogen highly reversible and fast since no structural change occurs in the framework [35]. The pore size of

MOFs can be tailored to increase the interaction of hydrogen. It is reported that the optimum pore size can range up to 6 Å that can lead to the maximum interactions among the hydrogen-framework. Other than this, catenation is also reported to reduce pore size in the MOFs to increase the uptake of hydrogen. Further, doping the alkali metals has also been reported to increase the efficiency of MOFs to take hydrogen. [36] Furthermore, it has been observed that hydrogen uptake in MOFs at cryogenic temperatures is very promising and quite significant at room temperatures. Until now, the highest storage capacity for hydrogen is reported to be 99.5 mg/gm at 56 bar pressure and a temperature of 77K for MOF NU-100 [37]. Despite the good efficiency of MOFs there is still a long way to go to synthesize practical hydrogen storing MOFs for everyday use. Porous materials are an ideal candidate to store hydrogen. Among them, porous carbons, carbon nanofibers, nanotubes and activated carbons are the centre of the research [38]. The porous carbons can be obtained from either synthetic precursors or natural carbons sources such as coal, wood etc. The pore size is then tailored to increase the uptake of hydrogen. Among the various porous carbons, activated carbons are a promising material for hydrogen absorption due to the large surface area of 3000 m² g⁻¹ [39]. It has been reported that activated carbons can uptake Hydrogen ranging 0.2-5.5 wt. %. The capacity of porous carbons needs to improve to maximize the storage of H₂ in them. In order to overcome the needs for automobile fuel, hydrogen can act as a fuel source by storing in a fuel cell. However, the biggest hindrance in using hydrogen as a fuel in cars is its storage inside the vehicle. Storage of hydrogen chemically can provide a solution to these problems.

Apart from other storage materials, metal hydrides are also under the research. The metal hydrides store hydrogen via chemisorption. High storage capacities for hydrogen are shown by certain light metal hydrides such as MgH₂ shows a gravimetric capacity of 7.6 wt. % however, the main disadvantage of MgH₂ is that it requires a high temperature of 573 K to discharge the stored hydrogen and a high reactivity towards air and oxygen [32]. Similarly, complex metal hydrides of aluminium are also under research for hydrogen storage. Aluminium hydride AlH₃, alane has shown a hydrogen storage capacity of 10.1 wt.% [40]. Lithium alanates (LiAlH₄) are attractive hydrogen storage materials but it has an extremely high equilibrium pressure of hydrogen and is highly unstable. The hydride undergoes the following two step reaction kinetics to give hydrogen,



The above reactions give hydrogen at temperatures of 160°-200°C. Reaction (I) gives 5.3wt % Hydrogen while reaction (II) gives 2.65 wt. % hydrogen. Still 2.65 wt. % hydrogen is still unreleased which can be desorbed from the hydride at an elevated temperature of 680°C. Thus, this high temperature desorption and absorption of hydrogen has hindered the commercial use of lithium based hydrides [41]. The storage capacities of various light metal hydrides has been summarized in the table below.

Table 2 List of Alkali and Alkaline Earth metals with their Hydrogen Storage Capacities

Metal Hydride	Storage Capacity (wt. %)
LiH ₄	7.7
LiBH ₄	8.6
LiAlH ₄	7.3
NaH	4.9
NaBH ₄	7.3
NaAlH ₄	6.4
MgH ₂	6.3

At present, Sodium Alanates has been reported to show a theoretical 5.5 wt. % storage capacity for hydrogen although in actual only 5 wt. % is observed [42] The lack of storage medium for hydrogen has directed the research towards zeolites which are now being investigated for potential hydrogen storage. The zeolites are Aluminosilicate materials with large pores which act as molecular sieves [43]. The pore size of the zeolites can be manipulated to use them for hydrogen storage. It has been reported that only a small amount of hydrogen can be stored in zeolites (<0.3 wt. %) at room temperature or at temperature greater than 200 °C [44]. The maximum uptake of hydrogen 1.81 wt. % was observable for zeolite NaY at -196°C/ 15 bar. Zeolites are low cost, efficient hydrogen storage materials [45]. Alloys can be effectively used as catalysts, storage materials and other applications. The properties of such alloys depend on their morphologies, compositions and porosity.[46]. The recently synthesized and studied 2D and 3D porous nanoalloys have achieved considerable attention for their vast applications as

energy storage materials and fuel cells. The porosity can be created using certain pore forming agents during the synthesis such as Citric Acid. These pores can be used to store hydrogen in them which can serve as an alternative energy source. [47] High entropy alloy concept was presented by Yeh et. al in 2004. High entropy alloys can be defined as alloys which are formed by mixing five or more metals in equimolar ratios to form a solid solution [48] . Such materials can be used to store hydrogen and these are economical as well. A high entropy alloy of HfNbTiVZr was studied for its hydrogenation properties at different temperature-pressure conditions. The alloy was reported to absorb large amounts of Hydrogen with a reversible storage observed at 500 °C. The storage of hydrogen was facilitated by the internal strains [49]. Another HEA of $\text{CoFeMnTi}_x\text{V}_y\text{Zr}_z$ was reported to show room temperature hydrogen absorption capacity of 1.6 wt. % [50]. LaNiFeVMn HEA was reported to absorb 0.24-0.87 wt. % hydrogen in vacuum. Thus, multicomponent alloys present a prospect in storage of hydrogen for renewable energy. [51] Hydrogen being an abundant element can act as alternate for fossil fuels. There are numerous advantages of using hydrogen as a fuel since it is an environmental-friendly and non-polluting source [52]. However, research is still ongoing to produce such economical and efficient materials to store and transport hydrogen safely. Bimetallic systems have been extensively studied for their hydrogen properties. Pd-Au system has been studied for its hydrogen properties through the deposition of Pd atoms onto an Au crystal followed by annealing [53]. Other than the transition metal alloys, light-metal bimetallic alloys have also been investigated for their hydrogen capacity. An alloy of AlLi was reported to show more than 5.5 wt. % hydrogen capacity which is close to the target given by the Department of Energy (DOE) [54]. Hydrogen is an efficient fuel source and an alternative to the fossil fuels. However, the worldwide acceptability of hydrogen as a fuel solely depends upon the synthesis of improved storage materials for hydrogen and fuel cells [55]. An ideal cell or storage material should possess high stability, high capacity and low cost. Various alloys are being investigated for hydrogen absorption/desorption applications including alloys of Pd, Pt, and Ti etc.

2.2 Metal Nanoparticle synthesis by Partial Film Boiling Method

An environment friendly and efficient method for the synthesis of metal nanoparticles has been reported. The approach of partial film boiling or the Leidenfrost method were applied for the successful synthesis of porous nanoparticles of Pt and Pd. Two important strategies were explored in the synthesis. The nanoparticle precursors were reduced in the absence of any reducing agent such as ethanol by only using the film boiling method. Furthermore, it was

observed that in the presence of mild reducing agents such as citric acid and ethanol, Pt and Pd underwent reduction to nanoparticles. Citric acid not only acted as a reducing agent along with ethanol but also played the role of a stabilizing agent for the nanoparticles. The solution of Pd precursor ($\text{Pd}(\text{NO}_3)_2$) when placed on a superheated plate above 270°C floated with evaporation, turning into a black coloured flake. These flakes after drying were collected as Pd nanoparticles. The TEM analysis of the particles showed a diameter of 2-5nm. The specific surface area was around $54\text{ m}^2/\text{gm}$ as estimated through BET. In the second method, hot rod-type heater was immersed into the solution containing weighed amounts of citric acid and $\text{Pd}(\text{NO}_3)_2$ in distilled water. Ethanol was added in this superheated solution and boiled for 10 minutes. After removing the rod-type heater, the solution was boiled to remove the solvent at 80°C . Calcination in air atmosphere was done at 500°C to obtain the porous Pd Nanoparticles [56].

2.3 Leidenfrost Approach-Green Chemistry

Metal nanoparticles have also been synthesized using the green chemistry approach. Activated carbon supported Pd catalysts have been reported for the room temperature decomposition of formic acid without employing any toxic reducing agent using Leidenfrost reactors. An easy synthesis of Pd nanoparticles is reported by dripping Pd nitrate solution over a hot plate which leads to reduction to Pd NPs. These Pd NPs may be converted to PdO in atmospheric conditions. To study the formic acid decomposition, the prepared PdO catalyst was mixed with a solution of formic acid, water and triethylamine. This led to the reduction of PdO to active Pd catalyst that produced a significant amount of H_2 and CO_2 . However, the unsupported metal catalyst showed very poor catalytic activity which could be enhanced by using porous supported catalysts. Thus, the Leidenfrost approach has been extended to the synthesis of supported metal catalyst by following the same procedure. Activated carbon supported Pd NPs were prepared using the same experiment. The Leidenfrost droplet reactors do not need any reducing agents or high temperature calcinations and is an eco-friendly straightforward method of synthesis [57]. Oxide mesoparticles (CuO) have been reported by using the green chemistry approach of Leidenfrost method which find applications in solar energy, thermal imaging, photovoltaics and others [2].

2.4 Inverse Leidenfrost Effect for Nanoalloy synthesis

The inverse Leidenfrost method can be effectively applied to synthesize porous metal nanoparticles. The inverse Leidenfrost method was investigated by Song et.al [58] during the vitrification of the liquid droplet when dropped on to a cold medium such as liquid nitrogen. Vitrification can be defined as a phase transition where a liquid changes to an amorphous state without proper crystallization.

2.5 Use of Porous Nanoalloys for Energy Storage and Conversion

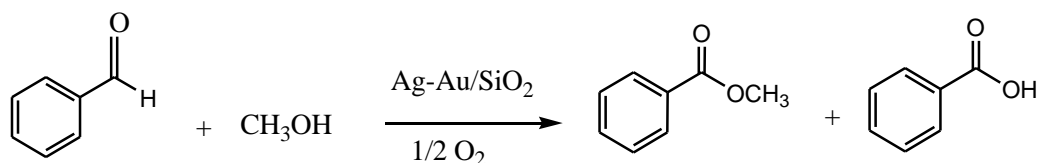
In recent times, porous alloys have found significant applications as materials for energy storage and energy conversion like alcohol oxidation, water splitting and hydrogen storage. A PtCuNi based porous nanoalloy has been reported which showed high catalytic activity for methanol oxidation [59]. The fuel cell showed greater efficiency than the bimetallic PtCu alloy and commercial Pt black. Similarly, porous PtPdCu electrocatalysts are also reported for methanol oxidation. The superior catalytic activity of these nanoalloys is due to their porous structure [60]. In Ag-Pd system a hydrogen permeable membrane is formed when Ag and Pd are in the ratio of 24:76 [61]. Pressure-composition isotherms were studied to investigate the hydrogen storage property of Ag-Rh Nanoparticles. The alloy Ag₅₀Rh₅₀ showed a maximum hydrogen absorption of 0.09 H/M at 100kPa [62].

2.6 Use of Ag-Au Nanoalloys as Catalysts

Catalysts are the vital part of chemical processes. Heterogeneous catalysis has achieved much attention now due to the easier metal recovery and environment friendly nature. Bimetallic NP catalysts possess remarkable electrical, magnetic and catalytic properties. Au and Ag NPs present a great opportunity for sustainable catalysis [63]. Gold and silver when used together show highly improved chemical stability and catalytic activity. One of the reasons for improved activity can be their lattice constants since Ag and Au both have almost same lattice constant (Ag=4.086 Å and Au=4.078Å).

Silver-Gold nanoalloys have been extensively used as catalysts for various organic and inorganic reactions. One such reaction is the oxidation of benzaldehyde reported [29]. The Ag-Au was prepared by the method of chemical reduction. The metal precursors (silver nitrate and chloroauric acid) were reduced by employing NaBH₄, a reducing agent. The catalysts produced

were characterized using various techniques such as UV-Vis, FTIR, XRD, SEM etc. The NPs produced were stabilized by supporting them over silica. Nanoalloys containing different proportion of Ag were synthesized by varying the concentrations of AgNO₃ solution. (1-2 wt. %). However, 1.5:1.5 wt. % Ag-Au showed the maximum efficiency for the oxidation of benzaldehyde using methanol as a solvent. The following reaction was observed:



Equation 1 Oxidation of Benzaldehyde using AgAu/SiO₂

Recently, the synthesis of supported bimetallic Ag-Au Nano catalysts have attracted much attention and various methods of synthesis have been devised such as chemical reduction, seed-growth, galvanic replacement reaction etc. Such alloys when supported with substrate like silica can be used for the preferential oxidation of CO reaction [64]. This can be ultimately used as a fuel. AgAu mesocomposites have been prepared and studied for the reduction of nitroaromatics including nitrobenzene and nitroacetophenone. The catalyst showed high catalytic activity as compared to the monometallic metals [65]. The hydrogen interaction with metal surfaces is important in heterogeneous catalysis. The bimetallic systems show various interactions with hydrogen. PdAu bimetallic system has been investigated for its number of applications such as hydrogen peroxide synthesis and degradation of hydrocarbons to produce hydrogen. Pd has the property to absorb as well as adsorb hydrogen into it. The PdAu system was subjected to temperature-programmed desorption of hydrogen to study the interactions built between the two. Au however, bonds weakly to hydrogen as compared to Pd [53].

2.7 Optical Properties of AgAu NPs

Alloying greatly affects the chemical stability in comparison to the pure metals. Wilcoxon et.al has studied the optical absorption properties for Ag and Au NPs and NAs [66]. The NAs of Au and Ag are miscible and possess the same lattice constants. Ag-Au nanoalloys were synthesized using 0.1 M HAuCl₄ and 0.1 M AgBF₄ by dissolving in 0.1 M TOAC (Tetraoctylammonium chloride) and toluene to make a micellar solution. The nanoalloys obtained were in Nano range of 3.1-5.5 nm. The prepared NAs were characterized for their optical absorbance and compared

with those of Ag and Au NPs.

Other than their excellent catalytic properties, the AgAu nanoparticles show remarkable optical properties being investigated by Rodriguez et.al [67]. The high chemical stability of Ag and Au has attributed this property to them. Multilayer nanoparticle alloy was synthesized by reducing salts of the metals (AgNO_3 and HAuCl_4) along with CTAB (cetyltrimethylammonium bromide). Gold NPs showing spherical geometry of the size=17nm were prepared which were coated with Ag and subsequently with another layer of Au. The finally obtained NPs were studied for their optical properties using the conduction electrons. The colour changes in the nanoparticles were observed in the visible region of the electromagnetic spectrum.

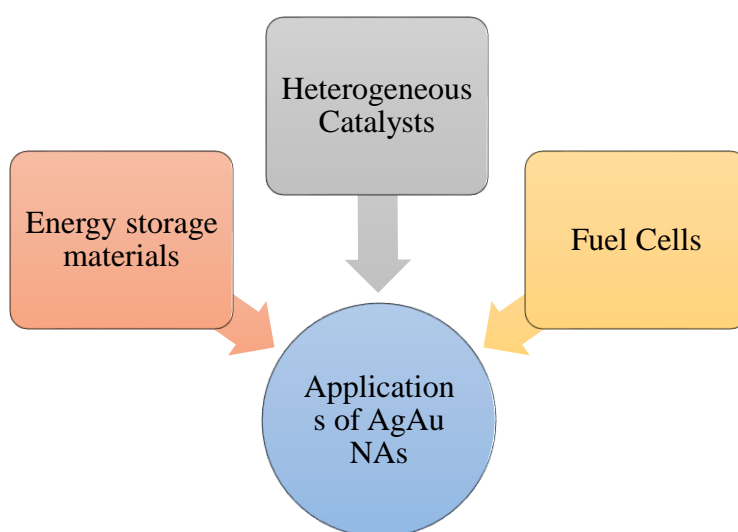


Figure 4 Applications of AgAu NAs

Chapter 3

EXPERIMENTAL

3.1 Experimental

This section includes chemicals and the methodology for the synthesis of AgAu nanoalloy.

3.1.1 Materials

Silver Nitrate (AgNO_3) and Citric acid were purchased from Sigma-Aldrich and used as such without any further purification. Pure gold was purchased from the market which was converted to HAuCl_4 . Deionized water was used for the synthesis.

3.2 Preparation of HAuCl_4

To 0.998 gm of gold metal 70 mL of Aqua Regia was added slowly in a china dish. The solution was brought to a temperature of 50°C using a hot plate with continuous stirring to allow the dissolution of gold metal. After the metal was completely dissolved, the temperature of the solution was raised to $70\text{--}80^\circ\text{C}$. The solution was boiled off until concentrated to approx. 30 mL. To this hot solution, more concentrated HCl was added to allow HNO_3 to evaporate. Brown fumes of HNO_3 were visible. This process was repeated until no more brown fumes of nitric acid appeared. The solution was further concentrated down to 15 mL and stored when cool. This solution of HAuCl_4 was used for further reaction.

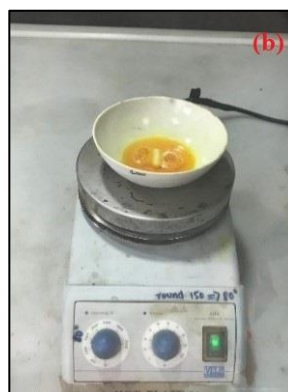
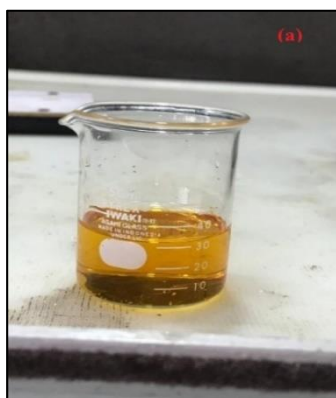


Figure 5 (a) Aqua Regia prepared to dissolve gold metal (b) Preparation of HAuCl_4 from gold

3.3 Synthesis of Macroporous AgAu Nanoalloy:

0.42 gm 2.4 (mmol) of AgNO_3 and 0.33 g (0.917 mmol) of HAuCl_4 was dissolved in a 400 mL of deionized water. 2 g (104 mmol) of citric acid was added into it. The mixture was boiled for 10 minutes. A properly insulated, hot rod-type heater was then immersed into the boiling solution. The temperature of the solution was arose abruptly to 230°C around the hot rod. This superheated state was maintained for 15 minutes. After this, 15ml of Ethanol was added into the solution by three equal portions as a reducing agent. The heating was continued with the hot rod for another 10 minutes followed by the removal of the hot rod. All the remaining solvent was evaporated on a water bath to obtain black solid mass. The residual mass was calcined at 500°C to obtain macroporous nanoalloy. Fig.8 represents the step by step synthesis of the AgAu nanoalloy. The final sample obtained weighed 0.937gm.

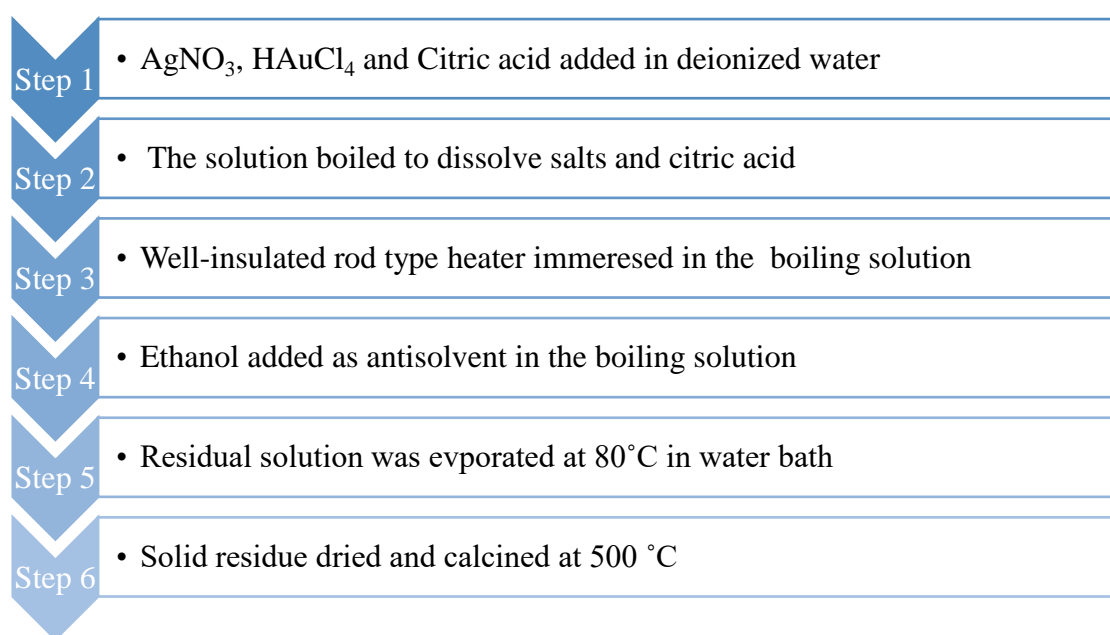


Figure 6 Step-by-step synthesis of AgAu NA



(a) Dissolution of precursor salts and citric acid in water



(b) Rod-type heater immersed in the boiling salt solution



(d) Solid residue obtained after fine grinding



(c) Solid residue obtained after calcination

Figure 6 Synthesis of AgAu nanoalloy

3.4 Hydrogen Absorption Capacity

0.5gm of the AgAu alloy sample was taken in a 50 mL Schlenk tube fitted with an inert gas vacuum line Fig 10 (a). The sample was degassed under vacuum by heating at 250 °C. The Schlenk tube was cooled to room temperature under vacuum and then dipped into a low temperature mixture containing both Acetone and liquid Nitrogen to attain a temperature of -78 °C (Fig. 10 (b)). A low temperature of -78°C was attained by using a mixture of Acetone and Liquid Nitrogen cooling bath. Since the freezing point of Acetone is -78°C, it was attained with the help of Liquid Nitrogen which has a freezing point of -197 °C. The extremely low temperature of liquid nitrogen froze the acetone mixture instantly. Hydrogen gas from a cylinder was allowed to enter into the Schlenk tube at -78°C for 3 hours. After this, the low temperature bath was removed and the Schlenk tube was allowed to reach the room temperature. The flow of hydrogen gas was stopped and this sample was sealed for further analysis.

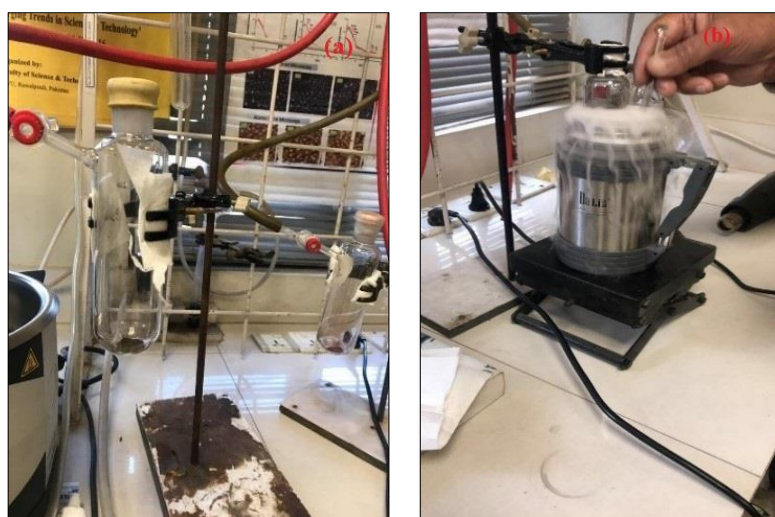


Figure 7 (a) Schlenk tube filled with AgAu sample under vacuum (b) Schlenk tube with AgAu sample submerged in Acetone/Liquid Nitrogen mixture

CHAPTER 4

RESULTS AND DISCUSSIONS

4.1 Hydrogen as an Alternate Energy Source:

Hydrogen is the most abundant element of the universe but a very small amount less than 1% is present in the form of molecular hydrogen. This 1% is chemically bonded in form of H₂O and other hydrocarbons. H₂O is the clean source of hydrogen energy that can be produced by electrolysis. After the successful use of hydrogen as a fuel in space technology, scientists all around the world are working on projects to use hydrogen as a safe and non-toxic fuel for everyday use. Hydrogen is an efficient alternate source of fuel. The main drawback in using hydrogen as a fuel is the lack of cheap and effective hydrogen storing materials. The lack of non-hazardous and benign hydrogen storage materials is the main drawback to the use of hydrogen as fuel. The search of such a hydrogen storage material is the target of our research. Bimetallic porous nanoalloys can be effectively used as hydrogen storage materials. In this research, AgAu bimetallic alloy has been synthesized which was studied for its hydrogen absorption capacity. Gold metal purchased was converted to H₂AuCl₄ by a simple method investigated by De Souza et.al [68]. Veit et.al suggested that aqua Regia is usually used as a laboratory solvent to dissolve gold but is not applicable at the industrial level. [69]. Aqua Regia is used to “digest” noble metals such as Au and Pd. The only disadvantage of pure aqua Regia is its corrosive nature. [70] Aqua Regia or “Royal Water” was prepared by mixing three parts 35 % hydrochloric acid (HCl) with one part 65% Nitric Acid (HNO₃). HCl or HNO₃ alone cannot dissolve gold as both of them behave differently. The HNO₃ present acts as an oxidizing agent and converts Au to Au⁺³ ions. The HCl plays its part by donating the Cl⁻ ions to the Au⁺³ ion to form tetrachloroaurate (III). This is an equilibrium reaction favouring the formation of AuCl₄⁻ which causes the oxidation of more gold to gold ions in the solution. The whole reaction was carried out in a fume hood. 35 ml of HCl was mixed into 15 ml HNO₃ to get 50 ml Aqua Regia which was stored in amber coloured bottle. This prepared aqua Regia was used to prepare H₂AuCl₄.

4.2 XRPD Results

The X-ray powder diffraction analysis was performed to investigate the phase and crystal structure of the alloy as well as particle size was calculated. The X-ray diffractogram obtained showed peaks at (111), (200), (220), and (311) which corresponded to the peak positions of 38.12, 44.30, 64.45 and 77.49 respectively (Figure 10). These peaks confirmed the fcc structure for the synthesized AgAu NA [71]. However, due to oxidation of Ag to Ag₂O peak was observed at 32.16 (marked *) indexed to (111) [72]. The small peaks formed due to AgCl at peak positions of 46.26° and 67.50° correspond to the diffraction planes of (022) and (004) respectively. AgCl was formed when the precursor salts were mixed during the synthesis of the alloy. This AgCl is stable and did not decompose at 500°C. The remaining peaks maybe due to the presence of undecomposed carbonaceous content from citric acid and may be acting as a coating material to prevent further oxidation of Ag in the alloy.

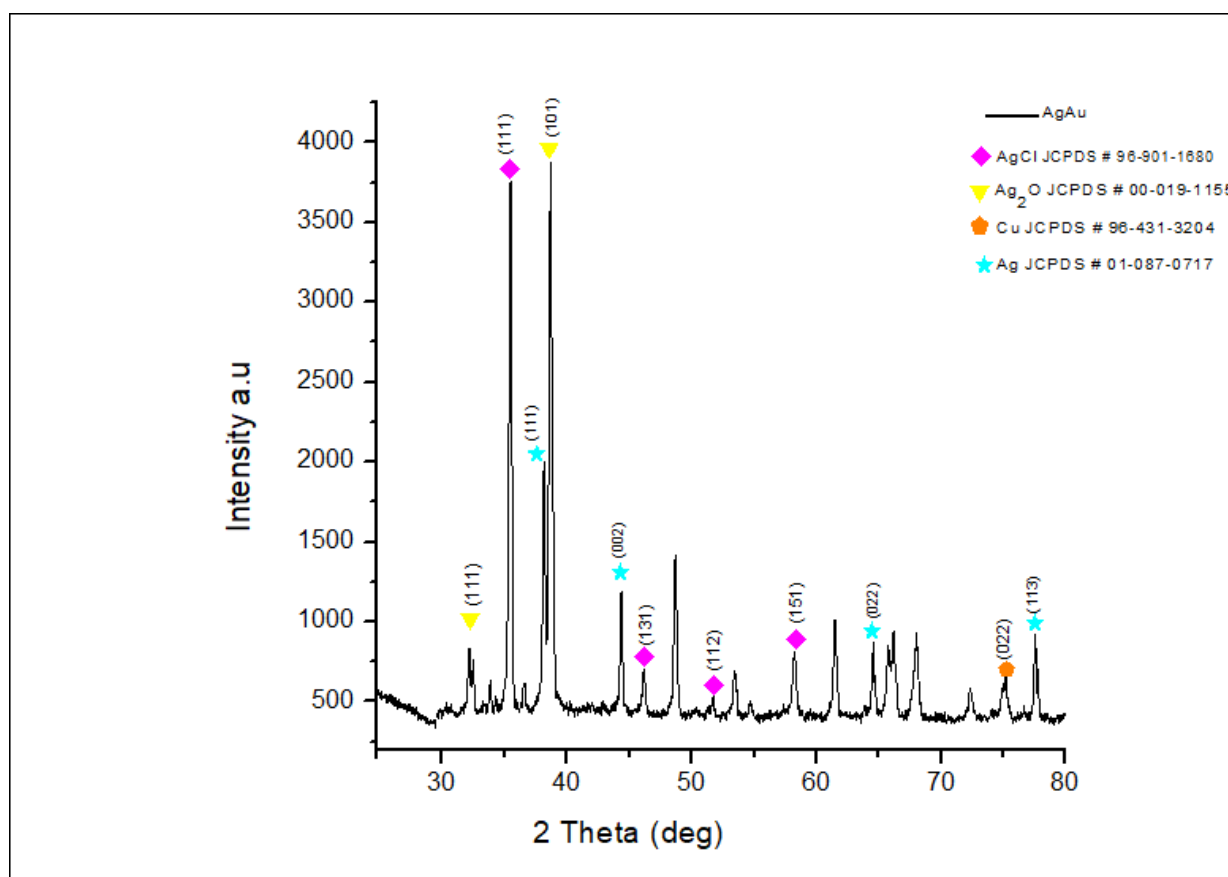


Figure 8 XRD patterns for AgAu alloy obtained after fine grinding

Sr. No	Peak Position [2 θ]	Theta [θ]	β	Crystallite Size (nm)
1	24.5591	12.27955	0.0037	37.44
2	25.1729	12.58645	0.0034	41.47
3	32.17	16.085	0.0108	13.24
4	35.464	17.732	0.0046	31.42
5	38.6966	19.3483	0.0052	27.76
6	44.3638	22.1819	0.0046	32.33
7	46.1847	23.09235	0.0077	19.46
8	48.6807	24.34035	0.0651	2.33
9	53.4068	26.7034	0.0075	2.04
10	58.2762	29.1381	0.0077	20.42
11	61.4883	30.74415	0.0062	25.72
12	64.5777	32.28885	0.0062	26.2
13	66.2144	33.1072	0.015	11.03
14	67.9944	33.9972	0.01	16.58
15	72.3727	36.18635	0.0088	19.52
16	75.1961	37.59805	0.0129	13.56
17	77.5489	38.77445	0.0037	48.05
Average size			22.85	

Table 3 Average Crystallite size obtained from the XRD pattern for AgAu

The crystallite size was calculated by employing the Debye-Scherrer [73] formula given as:

$$D = \frac{K\lambda}{\beta \cos\theta}$$

Where,

β = FWHM

λ =wavelength of the X-ray source used.

For Cu K α source, wavelength is set at 0.154nm.

$K=0.9$ (constant)

The Debye-Scherrer is a quick method for the calculation of the crystallite size although it has certain limitations. The β is known as Full Width at Half Maximum and its value depends on both the instrument as well as the micro strains in the structure. The crystallite size was calculated and average crystallite size is mentioned in the table 3. The average crystallite size was estimated to be 22.85nm.

4.3 SEM Results

Figure 11 shows the SEM images for AgAu nanoalloy particles of different sizes with most of them possessing a spherical geometry. It is observed that the alloy has an nm ranged pore size which can effectively take up hydrogen gas. Also the pores are attributed as structural defects within the alloy produced due to the pore forming agent. The pores show variable sizes ranging from 142-35 nm. The EDX spectrum also confirmed the presence of AgAu nanostructures. The prepared nanoalloy had the composition $Ag_{0.28} Au_{0.96}$ atomic percent. The peak for Carbon present in the EDX spectrum having an atomic percent composition of 12.77 % indicated the presence of carbon due to the citric acid present in the alloy which can be removed by sintering the alloy for longer duration at high temperatures. The peak for Cu having 3.95 atomic percent composition maybe due to the impurity in Au purchased commercially. Moreover, the 37.69 atomic percent Oxygen is incorporated since the reaction was performed in open atmospheric conditions. This can be reduced by providing inert atmospheric conditions. XRPD and SEM/EDX data showed the formation of AgAu nanoalloy. The SEM image along with the EDX spectrum is shown in the figure 10.

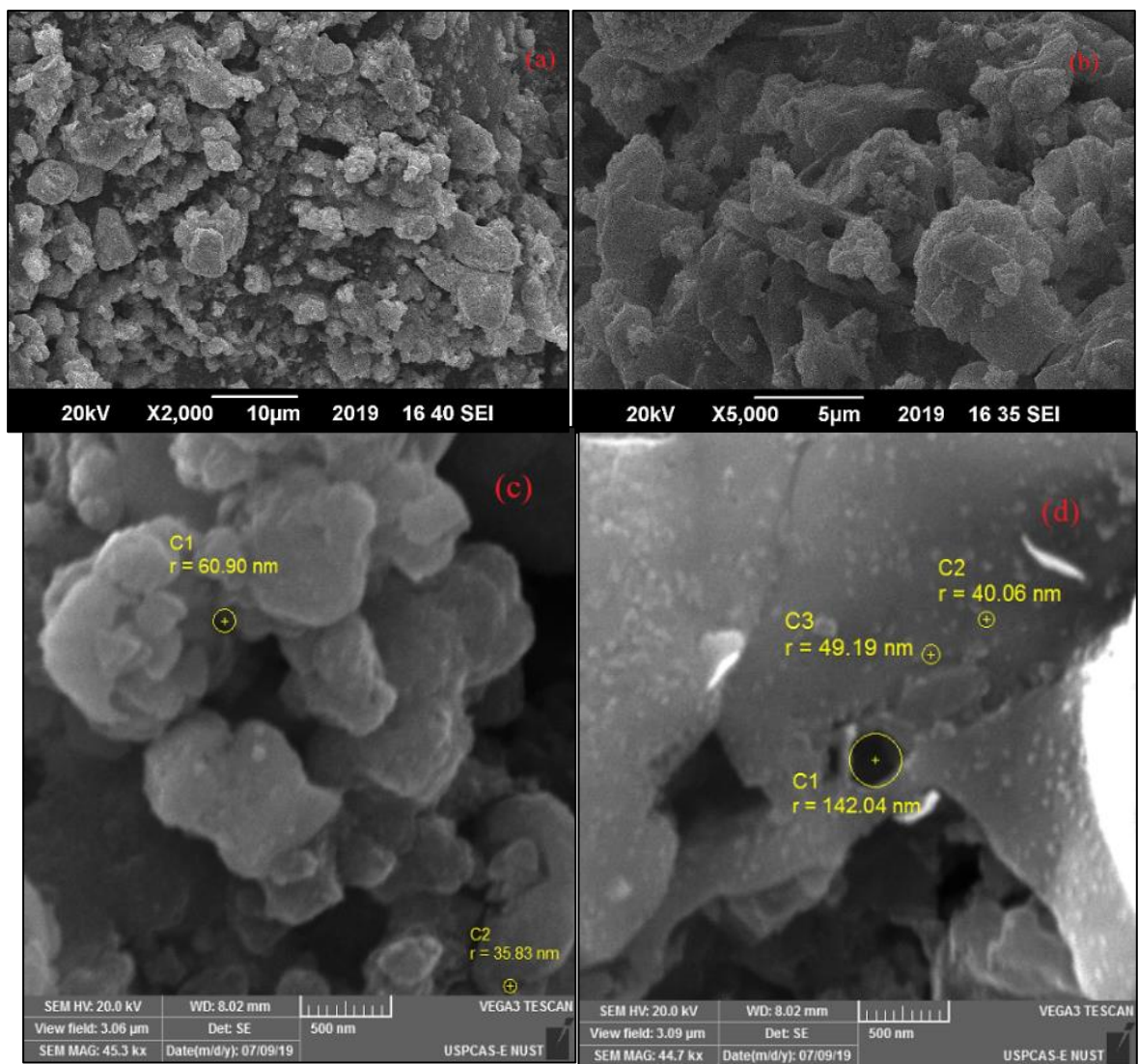


Figure 9 SEM images obtained for AgAu Nanoalloy at various magnifications (a) shows the overall morphology of the alloy with porous structure (b) a closer view showing large structural defects (c) size of the pore in nm range (d) large structural defect of 142 nm visible

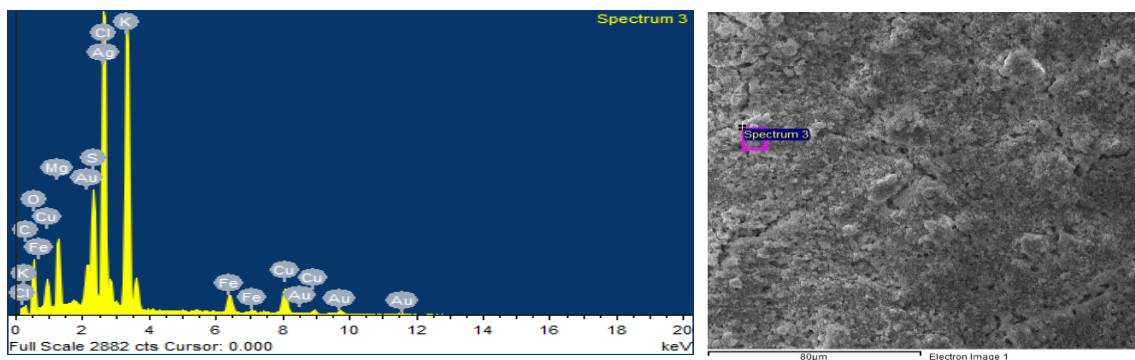


Figure 10 SEM micrograph of AgAu NA with EDX spectrum

4.4 FTIR Analysis

The FTIR is a tool to investigate the functional groups present. It can also be used to provide information about the catalyst surface [74]. The FTIR analysis was performed immediately after sintering the alloy at 500°C and also after absorption of hydrogen in the alloy. The FTIR graphs obtained for AgAu NAs was compared with FTIR graphs of AgAu bimetallic catalysts and that of pure Ag NPs and Au NPs. Figure 11 shows the FTIR spectrum for the as synthesized nanoalloy and obtained after sintering the alloy at 500 °C. The alloy was devoid of any moisture since no peak was observed around 3400 cm^{-1} . The peak observed at 1134 cm^{-1} can be attributed to the undecomposed citric acid.

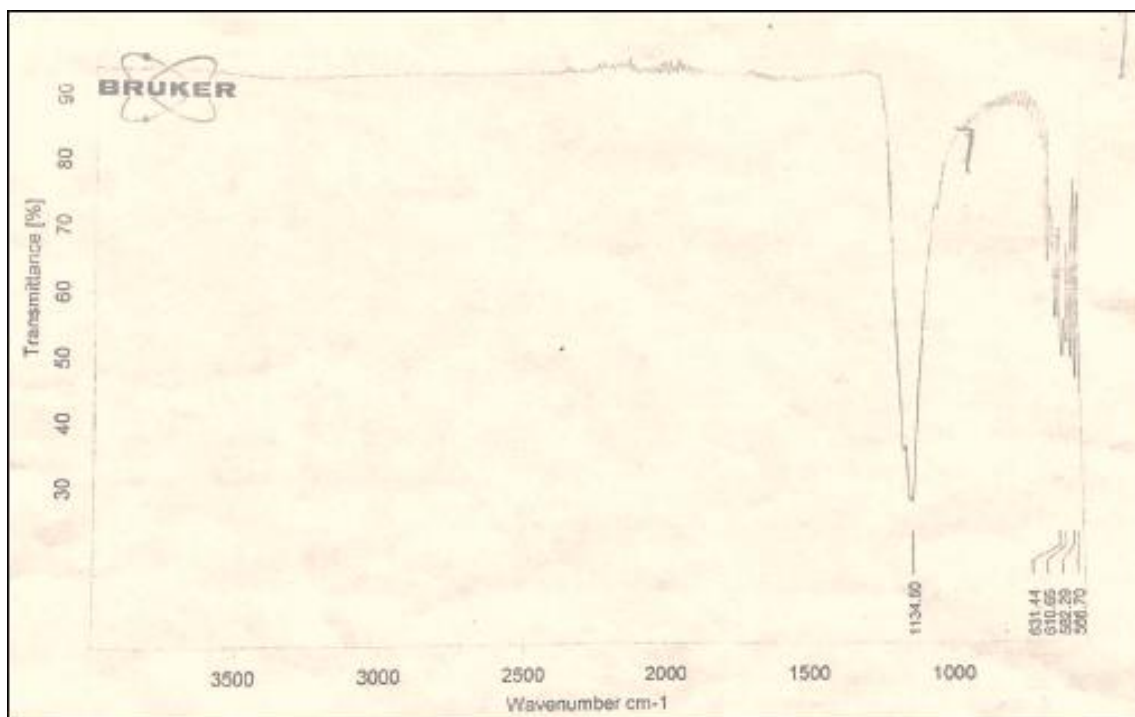


Figure 11 FTIR Spectrum of AgAu NA obtained after sintering at 500°C

The FTIR spectrum obtained after hydrogenation of the alloy at -78 °C showed peaks for AgAu bimetallic Nanoalloy (Fig. 12). The interaction of hydrogen with the metal is shown in 1400-2000 cm^{-1} of the spectrum. [75]

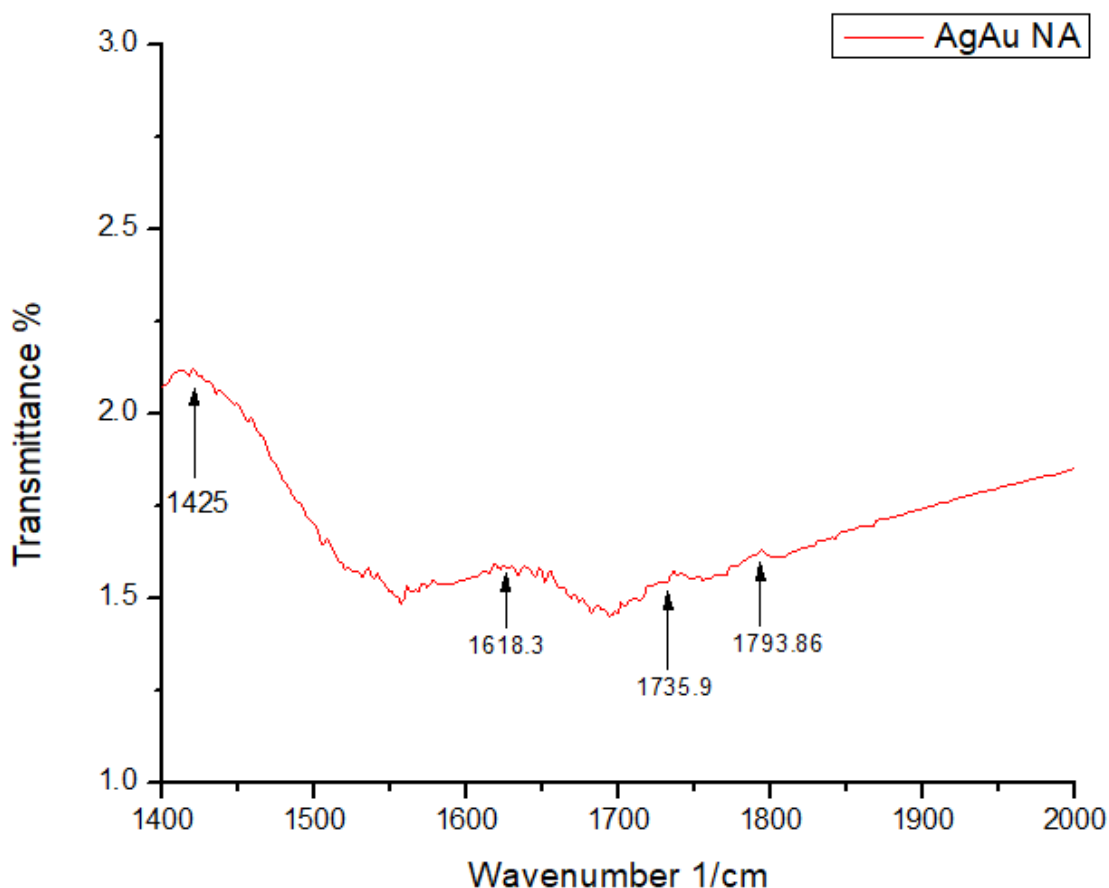


Figure 12 FTIR spectrum of AgAu NA after hydrogen absorption at $-78\text{ }^{\circ}\text{C}$

4.5 Thermogravimetric (TGA) Analysis

The thermogravimetric analysis was done to measure the weight change in the sample. The analysis was performed in Nitrogen atmosphere with the temperature raised up till $800\text{ }^{\circ}\text{C}$ with a rise of $10\text{ }^{\circ}\text{C}/\text{min}$. TGA before and after hydrogen absorption experiment has been analysed to investigate the mass losses in the alloy. Fig. 5 shows the TGA curve for the as-prepared alloy after sintering. The TGA curve obtained for the alloy showed it to be stable. Little mass loss was observed in the start which is attributed to the loss of any trapped moisture and volatile organic compounds in the alloy after which the material exhibited stable behaviour over a range of temperature. Overall the AgAu NA was not heat sensitive and showed stability.

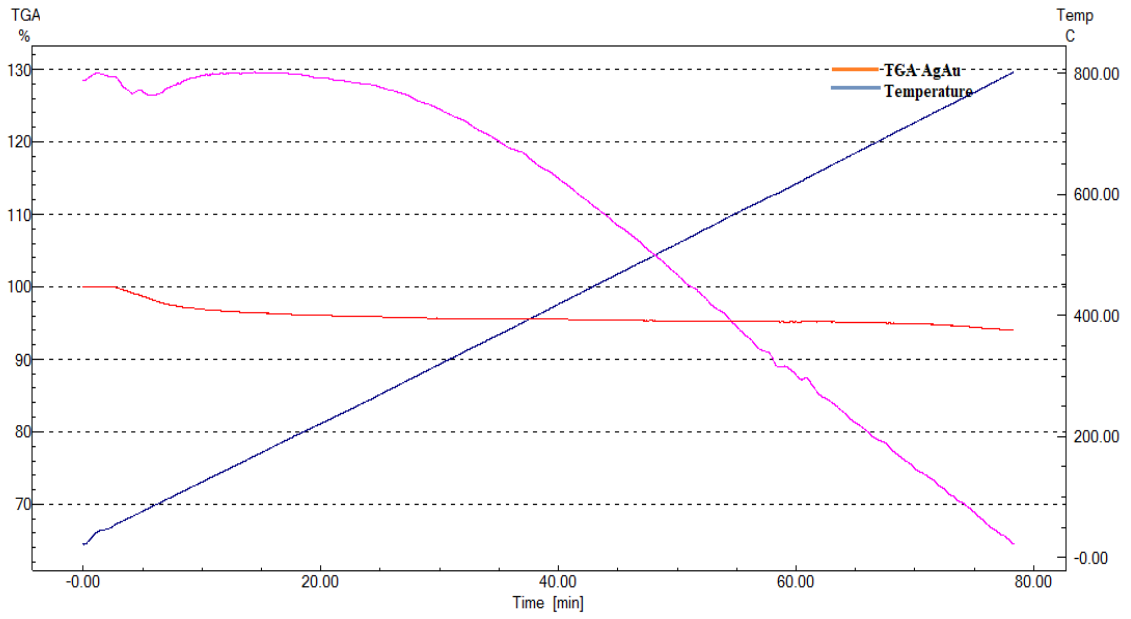


Figure. 13 TGA curve for AgAu nanoalloy after sintering at 500°C

After the absorption of hydrogen, the sample was subjected to Thermogravimetric analysis immediately to detect any hydrogen absorbed. The absorption could be detected the mass loss as the temperature is increased.

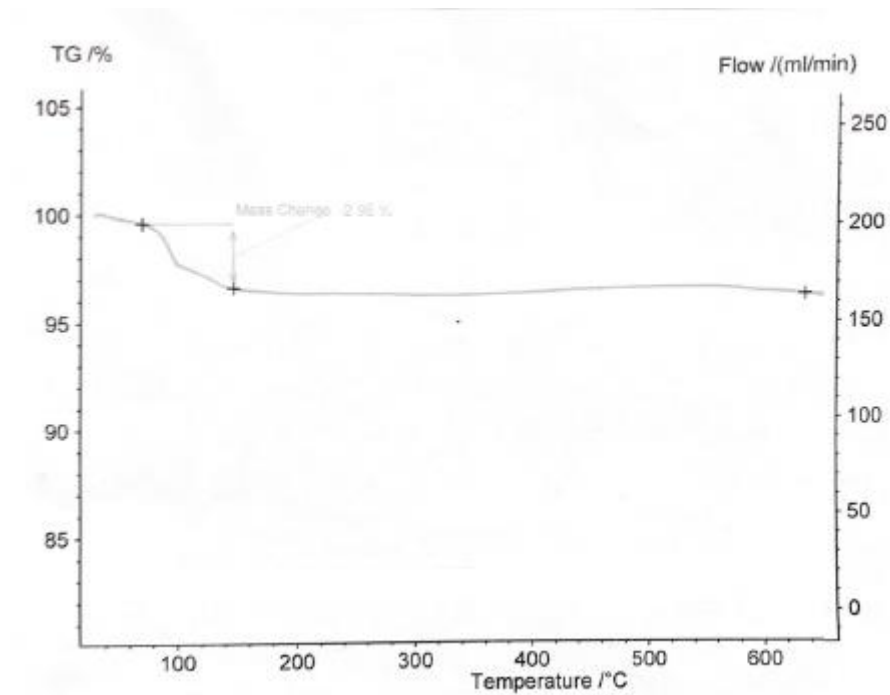


Figure 14 TGA curve showing mass loss after absorption of hydrogen for AgAu nanoalloy

The curve in the figure 14 represents the mass loss observed as the sample was heated to 600°C. As the sample approached 100°C, mass loss was observed in the sample. The total loss in mass was found to be 2.95% of the original weight of the sample. This mass loss can be attributed to the sorped H₂ which was desorped in the temperature range of 100°-175°C. Further heating the sample up to 600°C did not bring any change in the mass and the sample depicted stability [76].

4.6 Conclusion

AgAu nanoalloy has been synthesized using the inverse Leidenfrost method. The approach is novel, simple and economical. Since bimetallic alloys can serve as hydrogen storage materials, the prepared AgAu bimetallic alloy was studied for its hydrogen absorption capacity in view of the recent use of bimetallic catalysts for hydrogen energy. The alloy was characterized for its morphology, crystal structure, geometry and composition using XRPD, SEM/EDX and FTIR. XRD data showed peaks for both Ag and Au. The mass loss was indicated using TGA. The Thermal analysis showed a small mass change after hydrogen was absorbed in the nanoalloy which depicted its hydrogen absorption properties. The prepared alloy can be further modified for use as a hydrogen fuel cell. Using the simple inverse Leidenfrost approach, bimetallic catalysts for other metals can be prepared such as Pt, Cu and Ni etc. Furthermore, BET can be done to find out the porous surface area of the alloy prepared. The hydrogen absorption property of the alloy can be enhanced by doping it with other metals. Bimetallic alloys for hydrogen absorption are a new future for the renewable energy. They can be successfully tailored to store and transport hydrogen safely.

References

1. Furukawa, S. and T. Komatsu, *Intermetallic compounds: promising inorganic materials for well-structured and electronically modified reaction environments for efficient catalysis*. ACS Catalysis, 2016. **7**(1): p. 735-765.
2. Abdelaziz, M., et al., *Transflective Mesoscopic Nanoparticles Synthesized in the Leidenfrost Droplet as Black Absorbers*. Advanced Materials Interfaces, 2019. **6**(1): p. 1801610.
3. Gouda, E.S., *Classifications, characterization and applications of metallic alloys*. International Journal of Physics and Astronomy, 2014. **2**(2): p. 15-49.
4. Zhu, L., et al., *Substitutional alloy of Bi and Te at high pressure*. Physical Review Letters, 2011. **106**(14): p. 145501.
5. Hume-Rothery, W. and G. Raynor, *The structure of metals and alloys*, Institute of Metals. 1969, London.
6. Tilley, R.J. and R. Tilley, *Understanding solids: the science of materials*. 2004: Wiley Online Library.
7. West, A.R., *Solid state chemistry and its applications*. 2014: John Wiley & Sons.
8. Zhu, L., Wang, H., Wang, Y., Lv, J., Ma, Y., Cui, Q., ... & Zou, G, *Substitutional alloy of Bi and Te at high pressure*. Physical Review Letters, 2011: p. 106(14).
9. Jones, D.R. and M.F. Ashby, *Engineering materials 2: an introduction to microstructures and processing*. 2012: Butterworth-Heinemann.
10. Dinga, G.P., *Hydrogen: the ultimate fuel and energy carrier*. Journal of Chemical Education, 1988. **65**(8): p. 688.
11. Rosen, M.A. and S. Koohi-Fayegh, *The prospects for hydrogen as an energy carrier: an overview of hydrogen energy and hydrogen energy systems*. Energy, Ecology and Environment, 2016. **1**(1): p. 10-29.
12. Barber, D. and I.C. Freestone, *An investigation of the origin of the colour of the Lycurgus Cup by analytical transmission electron microscopy*. Archaeometry, 1990. **32**(1): p. 33-45.
13. McNamara, K. and S.A. Tofail, *10 Biomedical applications of nanoalloys*. Nanoalloys: From Fundamentals to Emergent Applications, 2013: p. 345.
14. Johnston, R.L., *Metal nanoparticles and nanoalloys*, in *Frontiers of Nanoscience*. 2012, Elsevier. p. 1-42.
15. Pittaway, F., Paz-Borbón, L. O., Johnston, R. L., Arslan, H., Ferrando, R., Mottet, C., Fortunelli, A., *Theoretical studies of palladium– gold nanoclusters: Pd– Au clusters with up to 50 atoms*.

- The Journal of Physical Chemistry C, 2009: p. Pittaway, F., Paz-Borbón, L. O., Johnston, R. L., Arslan, H., Ferrando, R., Mottet, C., ... & Fortunelli, A. (2009). Theoretical s113(21).
16. Sinfelt, J.H., & Cusumano, J. A., *Bimetallic catalysts*. 1983, Wiley.
 17. Leidenfrost, J.G., *De aquae communis nonnullis qualitatibus tractatus*. 1756: Ovenius.
 18. Antonini, C., Bernagozzi, I., Jung, S., Poulidakos, D., & Marengo, M., *Water drops dancing on ice: How sublimation leads to drop rebound*. Physical review letters, (2013): p. 111(1).
 19. Biance, A.-L., C. Clanet, and D. Quéré, *Leidenfrost drops*. Physics of Fluids, 2003. **15**(6): p. 1632-1637.
 20. Faraday, M., *On the relation of water to hot polished surfaces*. QJ Sci., Lit., Arts, 1828. **1**: p. 221.
 21. Hall, R., et al., *Inverse leidenfrost phenomenon*. Nature, 1969. **224**(5216): p. 266.
 22. Stuart, B., *Infrared spectroscopy*. Kirk-Othmer Encyclopedia of Chemical Technology, 2000: p. 1-18.
 23. Das, R., E. Ali, and S.B. Abd Hamid, *CURRENT APPLICATIONS OF X-RAY POWDER DIFFRACTION-A REVIEW*. Reviews on Advanced Materials Science, 2014. **38**(2).
 24. Haguenau, F., et al., *Key events in the history of electron microscopy*. Microscopy and Microanalysis, 2003. **9**(2): p. 96-138.
 25. Stadtländer, C., *Scanning electron microscopy and transmission electron microscopy of mollicutes: challenges and opportunities*. Modern research and educational topics in microscopy, 2007. **1**: p. 122-131.
 26. Vernon-Parry, K., *Scanning electron microscopy: an introduction*. III-Vs Review, 2000. **13**(4): p. 40-44.
 27. Price, D.M., D.J. Hourston, and F. Dumont, *Thermogravimetry of polymers*. Encyclopedia of Analytical Chemistry: Applications, Theory and Instrumentation, 2006.
 28. Loganathan, S., et al., *Thermogravimetric analysis for characterization of nanomaterials*, in *Thermal and Rheological Measurement Techniques for Nanomaterials Characterization*. 2017, Elsevier. p. 67-108.
 29. Vadakkekara, R., M. Chakraborty, and P.A. Parikh, *Room temperature benzaldehyde oxidation using air over gold-silver nanoalloy catalysts*. Journal of the Taiwan Institute of Chemical Engineers, 2015. **50**: p. 84-92.
 30. Shafiee, S. and E. Topal, *When will fossil fuel reserves be diminished?* Energy policy, 2009. **37**(1): p. 181-189.
 31. Ren, J., et al., *Current research trends and perspectives on materials-based hydrogen storage solutions: A critical review*. 2016.

32. Sakintuna, B., F. Lamari-Darkrim, and M. Hirscher, *Metal hydride materials for solid hydrogen storage: a review*. International journal of hydrogen energy, 2007. **32**(9): p. 1121-1140.
33. Broom, D., et al., *Outlook and challenges for hydrogen storage in nanoporous materials*. Applied Physics A, 2016. **122**(3): p. 151.
34. Khafidz, N.Z.A.K., et al., *The kinetics of lightweight solid-state hydrogen storage materials: a review*. International Journal of Hydrogen Energy, 2016. **41**(30): p. 13131-13151.
35. Panella, B. and M. Hirscher, *Hydrogen physisorption in metal–organic porous crystals*. Advanced Materials, 2005. **17**(5): p. 538-541.
36. Langmi, H.W., J. Ren, and N.M. Musyoka, *Metal–organic frameworks for hydrogen storage*, in *Compendium of Hydrogen Energy*. 2016, Elsevier. p. 163-188.
37. Farha, O.K., et al., *De novo synthesis of a metal–organic framework material featuring ultrahigh surface area and gas storage capacities*. Nature chemistry, 2010. **2**(11): p. 944.
38. De la Casa-Lillo, M., et al., *Hydrogen storage in activated carbons and activated carbon fibers*. The Journal of Physical Chemistry B, 2002. **106**(42): p. 10930-10934.
39. Xia, Y., Z. Yang, and Y. Zhu, *Porous carbon-based materials for hydrogen storage: advancement and challenges*. Journal of Materials Chemistry A, 2013. **1**(33): p. 9365-9381.
40. Paskevicius, M., et al., *Mechanochemical synthesis of aluminium nanoparticles and their deuterium sorption properties to 2 kbar*. Journal of alloys and compounds, 2009. **481**(1-2): p. 595-599.
41. Zaluski, L., A. Zaluska, and J. Ström-Olsen, *Hydrogenation properties of complex alkali metal hydrides fabricated by mechano-chemical synthesis*. Journal of alloys and compounds, 1999. **290**(1-2): p. 71-78.
42. Schüth, F., B. Bogdanović, and M. Felderhoff, *Light metal hydrides and complex hydrides for hydrogen storage*. Chemical communications, 2004(20): p. 2249-2258.
43. Dyer, A., *An introduction to zeolite molecular sieves*. 1988.
44. Beyaz Kayiran, S. and F. Lamari Darkrim, *Synthesis and ionic exchanges of zeolites for gas adsorption*. Surface and Interface Analysis: An International Journal devoted to the development and application of techniques for the analysis of surfaces, interfaces and thin films, 2002. **34**(1): p. 100-104.
45. Langmi, H., et al., *Hydrogen adsorption in zeolites A, X, Y and RHO*. Journal of Alloys and Compounds, 2003. **356**: p. 710-715.
46. Jiang, B., Li, C., Malgras, V., & Yamauchi, Y., *Synthesis of ternary PtPdCu spheres with three-dimensional nanoporous architectures toward superior electrocatalysts*. Journal of Materials Chemistry A, 2015: p. 3(35), 18053-18058.
47. Sakamoto, T., & Atsumi, H., *Hydrogen absorption/desorption characteristics of Mg-V-Ni hydrogen storage alloys*. Fusion Engineering and Design, 2019: p. 138, 6-9.

48. Yeh, J.W., et al., *Nanostructured high-entropy alloys with multiple principal elements: novel alloy design concepts and outcomes*. *Advanced Engineering Materials*, 2004. **6**(5): p. 299-303.
49. Karlsson, D., et al., *Structure and hydrogenation properties of a HfNbTiVZr high-entropy alloy*. *Inorganic chemistry*, 2018. **57**(4): p. 2103-2110.
50. Kao, Y.-F., et al., *Hydrogen storage properties of multi-principal-component CoFeMnTi_xVyZr_z alloys*. *international journal of hydrogen energy*, 2010. **35**(17): p. 9046-9059.
51. Kunce, I., M. Polański, and T. Czujko, *Microstructures and hydrogen storage properties of La Ni Fe V Mn alloys*. *Int. J. Hydrogen Energy*, 2017. **42**: p. 27154.
52. Cortright, R.D., R. Davda, and J.A. Dumesic, *Hydrogen from catalytic reforming of biomass-derived hydrocarbons in liquid water*, in *Materials For Sustainable Energy: A Collection of Peer-Reviewed Research and Review Articles from Nature Publishing Group*. 2011, World Scientific. p. 289-292.
53. Yu, W.-Y., G.M. Mullen, and C.B. Mullins, *Hydrogen adsorption and absorption with Pd–Au bimetallic surfaces*. *The Journal of Physical Chemistry C*, 2013. **117**(38): p. 19535-19543.
54. Zhong, M., C. Huang, and G. Wang, *Hydrogen storage of Al-Li bimetal alloy nanostructures*. *Journal of Alloys and Compounds*, 2017. **725**: p. 388-392.
55. Kumar, A., et al., *Hydrogen storage properties of Ti₂- xCrVM_x (M= Fe, Co, Ni) alloys*. *International Journal of Hydrogen Energy*, 2013. **38**(30): p. 13335-13342.
56. Lee, D.-W., et al., *Straightforward Synthesis of Metal Nanoparticles and Hierarchical Porous Metals Assisted by Partial Film Boiling Phenomena*. *Chemistry of Materials*, 2015. **27**(15): p. 5151-5160.
57. Lee, D.-W., et al., *Reducing-agent-free instant synthesis of carbon-supported Pd catalysts in a green Leidenfrost droplet reactor and catalytic activity in formic acid dehydrogenation*. *Scientific reports*, 2016. **6**: p. 26474.
58. Song, Y.S., Adler, D., Xu, F., Kayaalp, E., Nureddin, A., Anchan, R. M., Demirci, U, *Vitrification and levitation of a liquid droplet on liquid nitrogen*. *Proceedings of the National Academy of Sciences*, 2010: p. 4596-4600.
59. Lan, J., et al., *One-step synthesis of porous PtNiCu trimetallic nanoalloy with enhanced electrocatalytic performance toward methanol oxidation*. *Journal of Saudi Chemical Society*, 2019. **23**(1): p. 43-51.
60. Jiang, B., et al., *Synthesis of ternary PtPdCu spheres with three-dimensional nanoporous architectures toward superior electrocatalysts*. *Journal of Materials Chemistry A*, 2015. **3**(35): p. 18053-18058.
61. Holleck, G.L., *Diffusion and solubility of hydrogen in palladium and palladium--silver alloys*. *The Journal of Physical Chemistry*, 1970. **74**(3): p. 503-511.

62. Kusada, K., et al., *Hydrogen-storage properties of solid-solution alloys of immiscible neighboring elements with Pd*. Journal of the American Chemical Society, 2010. **132**(45): p. 15896-15898.
63. Devarajan, S., P. Bera, and S. Sampath, *Bimetallic nanoparticles: a single step synthesis, stabilization, and characterization of Au–Ag, Au–Pd, and Au–Pt in sol–gel derived silicates*. Journal of colloid and interface science, 2005. **290**(1): p. 117-129.
64. Liu, X., et al., *Synthesis of Au–Ag alloy nanoparticles supported on silica gel via galvanic replacement reaction*. Progress in Natural Science: Materials International, 2013. **23**(3): p. 317-325.
65. Sareen, S., et al., *Synthesis of bimetallic Au–Ag alloyed mesocomposites and their catalytic activity for the reduction of nitroaromatics*. Applied Surface Science, 2018. **435**: p. 552-562.
66. Wilcoxon, J., *Optical Absorption Properties of Dispersed Gold and Silver Nanoparticles*. Journal of Physical Chemistry B, 2009: p. 2647-2656.
67. Rodríguez-González, B., et al., *Multishell bimetallic AuAg nanoparticles: synthesis, structure and optical properties*. Journal of Materials Chemistry, 2005. **15**(17): p. 1755-1759.
68. De Souza, C.D., B.R. Nogueira, and M.E.C. Rostelato, *Review of the methodologies used in the synthesis gold nanoparticles by chemical reduction*. Journal of Alloys and Compounds, 2019.
69. Veit, H.M., et al., *Recovery of copper from printed circuit boards scraps by mechanical processing and electrometallurgy*. Journal of hazardous materials, 2006. **137**(3): p. 1704-1709.
70. Elomaa, H., et al., *The effect of the redox potential of aqua regia and temperature on the Au, Cu, and Fe dissolution from WPCBs*. Recycling, 2017. **2**(3): p. 14.
71. Zhang, Y., et al., *Chloroplasts-mediated biosynthesis of nanoscale Au–Ag alloy for 2-butanone assay based on electrochemical sensor*. Nanoscale research letters, 2012. **7**(1): p. 475.
72. Dhoondia, Z.H. and H. Chakraborty, *Lactobacillus mediated synthesis of silver oxide nanoparticles*. Nanomaterials and nanotechnology, 2012. **2**: p. 15.
73. Scherrer, P., *Bestimmung der inneren Struktur und der Größe von Kolloidteilchen mittels Röntgenstrahlen*, in *Kolloidchemie Ein Lehrbuch*. 1912, Springer. p. 387-409.
74. Wei, Z., et al., *Bimetallic catalysts for hydrogen generation*. Chemical Society Reviews, 2012. **41**(24): p. 7994-8008.
75. Moshfegh, M., et al., *Biological synthesis of Au, Ag and Au–Ag bimetallic nanoparticles by α -amylase*. Dig. J. Nanomater. Bios, 2011. **6**: p. 1419-1426.
76. Feng, J.-J., et al., *Bimetallic AuPt alloy nanodendrites/reduced graphene oxide: One-pot ionic liquid-assisted synthesis and excellent electrocatalysis towards hydrogen evolution and methanol oxidation reactions*. International Journal of Hydrogen Energy, 2017. **42**(2): p. 1120-1129.